Journal of Materials Chemistry C

Accepted Manuscript

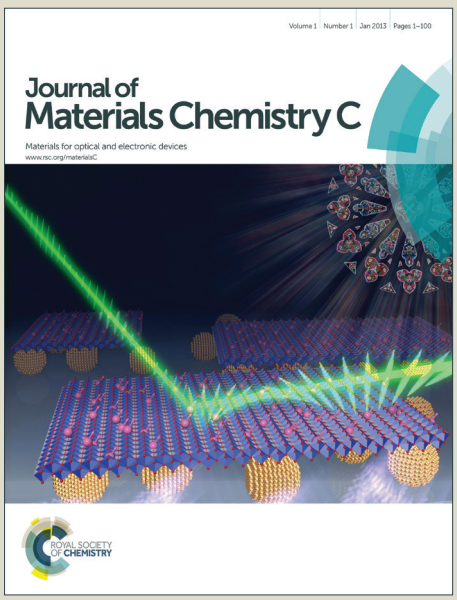

ROYAL SOCIETY OF CHEMISTRY

www.rsc.org/materialsC

Effective medium theory based modeling of the thermoelectric properties of composites: Comparison between predictions and experiments in the glass-crystal composite system $Si_{10}As_{15}Te_{75}$-$Bi_{0.4}Sb_{1.6}Te_3$

J-B. Vaney[1,2], A. Piarristeguy[2], V.Ohorodniichuck[1], O.Ferry[1], A.Pradel[2], E.Alleno[3], J.Monnier[3], E.B.Lopes[4], A.P. Gonçalves[4], G.Delaizir[5], C.Candolfi[1], A.Dauscher[1], B.Lenoir[1]

[1]*Institut Jean Lamour (IJL), UMR 7198 CNRS-Université de Lorraine, France*

[2]*Institut Charles Gerhardt (ICG), UMR 5253 CNRS-Université Montpellier 2, France*

[3]*Institut de Chimie et des Matériaux de Paris Est (ICMPE), UMR 7182 CNRS, CMTR, Thiais, France*

[4]*IST/ITN Instituto Superior Técnico, Universidade Técnica de Lisboa, P-2686-953 Sacavém, Portugal*

[5]*SPCTS, Université de Limoges UMR CNRS 7315, France*

Keywords

A. Glass-crystal composites

B. Thermoelectricity

C. Effective Medium Theory

Abstract

We report on the theoretical predictions of the Effective Medium Theory (EMT) and its generalized version taking into account percolation theory (GEMT) on the thermoelectric properties of composites based on Landauer and Sonntag's equations. The results were tested experimentally on composites composed of the glassy phase

$Si_{10}As_{15}Te_{75}$ and the crystalline phase $Bi_{0.4}Sb_{1.7}Te_3$. The evolution of the electrical resistivity and thermal conductivity with the fraction of crystalline phase matches very well the experimental data, although the GEMT model fails to predict the thermopower. A better agreement between theory and experiment could be obtained by combining the principles of the GEMT and the Webman-Jortner-Cohen models. Despite the fact that the GEMT model originally predicts the possibility to optimize the dimensionless figure of merit ZT of composites by adjusting the fraction and the values of the transport properties of each phase, the new model developed rules out any beneficial influence on the ZT values. These results confirm within a different framework the early conclusions of Bergman regarding the impossibility of improving the ZT values using multi-phased materials.

I. Introduction

In the current context of environmental concerns, energy harvesting has become a central focus in materials science research. Among all the technologies under scrutiny and development, thermoelectricity might play a role due to its numerous advantages such as the absence of gaseous emission, vibration-free character and versatility. However, for decades, the performance and efficiency of thermoelectric (TE) materials has been limited, confining them to niche applications and markets. Since the early 1990's, new strategies aimed to increase the efficiency of TE materials mushroomed, leading to a major rejuvenation of interest in this field of research [1, 2]. The thermoelectric performance of TE materials is quantitatively described by the dimensionless figure of merit defined as $ZT = \alpha^2.T/\rho.\lambda$, where α is the Seebeck

coefficient, T is the absolute temperature, ρ is the electrical resistivity and λ is the total thermal conductivity (the sum of the electronic and lattice contributions, λ_e and λ_L, respectively). Owing to the interdependence of these three transport properties, it appears extremely challenging to optimize one of them without impacting the others.

Among the various strategies explored, multi-phased materials proved to be a possible route towards high ZT values. Several studies were devoted to the investigation of materials that inherently show different nano-microstructures of various length scales referred to as all-scale hierarchical structures in literature [3-6]. Even though the thermal stability of these phases still remains to be thoroughly investigated, very high ZT values were reported in several lead chalcogenide-based materials. For instance, Biswas et al. reported a significant increase in ZT from 1.1 to 1.7 with the nano-precipitation of SrTe secondary phases inside an Na-doped PbTe matrix [3]. A similar strategy was applied to Na-doped PbSe compounds, with Ca-, Sr- or BaSe nano-precipitates, yielding a 30% increase [4]. Nanoparticles dispersion in a thermoelectric medium is considered as an interesting alternative to nano-precipitation and has been applied in conventional thermoelectric materials such as Bi_2Te_3-based alloys. In this regard, Li et al. reported on the effect of SiC nanoparticles dispersed in a Bi-Sb-Te matrix and observed an increase of 15% in ZT for as few as 0.4% of SiC particles [7]. All these optimizations arise from a significant decrease in the lattice thermal conductivity owing to numerous interfaces that act as efficient phonon diffusion centers.

So far, multi-phased materials composed of two different phases (none of them being at the nanometer length-scale) have been only scarcely studied. Chalcogenides or oxide glass-ceramics are examples of such materials, which, however, exhibit weak

thermoelectric performance (ZT < 0.2) [8, 9]. Even though recent investigations have demonstrated the possibility to enhance the thermoelectric properties of the glassy phase through the admixture of a small fraction of crystalline phase [10], the corresponding pure crystalline phase still displays higher performance than the glass-ceramics. These results seem to conform to the long-standing idea that possible enhancement of the power factor in composites is always at the expense of the overall performance *i.e.* an increase in ZT values is physically impossible as argued by Bergman and Fel [11]. Yet, their model took precisely into account neither percolation mechanisms nor interface effects, both of which likely playing a role in determining the transport properties in composites.

Herein, we predict the thermoelectric properties of composite materials composed of two different phases using both the effective medium theory (EMT) and its generalized derivation (GEMT) that takes into account elements of the percolation theory. Under specific conditions on the transport properties of the two phases, these models predict that the ZT values of composites might be optimized for a given volume ratio. In order to critically assess the validity of these models, we fabricated several two-phase composites with various volume ratios using the glassy $Si_{10}As_{15}Te_{75}$ and the crystalline $Bi_{0.4}Sb_{1.6}Te_3$ phases that fulfill the requirements of the model. The failure of these models to predict the evolution of the thermopower as a function of the crystalline fraction led us to introduce the Webman-Jortner-Cohen model, which yields a better agreement between theory and experiment.

The paper is organized in the following way. Experimental details concerning the fabrication and the measurements of the thermoelectric properties of the composites

are described in the first paragraph. The Effective Medium Theory (EMT) is then introduced together with its generalized counterpart (GEMT), providing a theoretical basis to choose the nature of the composite phases. The last part deals with the comparison of the model predictions and the experimental data.

II. Experimental details

The raw materials ($Si_{10}As_{15}Te_{75}$ glass and $Bi_{0.4}Sb_{1.6}Te_3$ crystalline phase) were prepared by two different synthesis routes. For glassy $Si_{10}As_{15}Te_{75}$, a total weight of 4 g of stoichiometric quantities of pure starting elements (Si 99.999% form Advent RM, As 99.99% from Goodfellow, Te 99.999% from 5NPlus) was placed and sealed in evacuated quartz ampules (6 mm inner diameter) under secondary vacuum (10^{-5} mbar). The ampules were then heated to 1023 K at a heating rate of 9 $K.h^{-1}$ and kept at this temperature for one hour. The tubes were regularly rocked in the furnace to ensure a good chemical homogenization. The tubes were finally quenched in a salt-ice-water mixture. The same procedure was rigorously followed for each sample to guarantee good reproducibility.

For $Bi_{0.4}Sb_{1.6}Te_3$, pure elements (Bi 99.999% from CERAC, Sb 99.999% from 5NPlus, Te 99.999% from 5NPlus) were placed and sealed in quartz ampules (14 mm inner diameter) under secondary vacuum (10^{-5} mbar), which were then heated to 953 K and kept at this temperature for 6 hours in an oscillating furnace. The ampules were quenched in room-temperature water to obtain the crystalline phase. XRD patterns of both phases are shown in Figure 1. The ingots were subsequently ground into powders

and finally consolidated into cylindrical pellets by SPS to ensure a better homogeneity in terms of crystal orientation.

Composites were fabricated for nine different volume ratios (crystalline/vitreous) from 10-90% up to 50-50% with an increasing step of 5%. Both materials were ground separately in agate mortars and sieved at 25 μm. For each sample, about 0.6 g of mixture of the two powders was then prepared abiding by the calculated volume ratios. The powder densification was performed by Spark Plasma Sintering (SPS), allowing for fast sintering in order to prevent the glass from crystallizing. The powders were densified at 408 K for 5 minutes under a pressure of 80 MPa. The evolution of the density of the composites according to the volume fraction of $Bi_{0.4}Sb_{1.6}Te_3$ is discussed in the electronic supplementary information (ESI).

Powder X-ray diffraction (PXRD) was performed at 300 K using a Bruker D8 Advance instrument with $CuK\alpha_1$ radiation. Selected composite samples were checked by scanning electron microscopy (SEM), using a Philips XL-30 SEM system in the back-scattering electron (BSE) mode (under 25 kV acceleration voltage) to determine their microstructure and the chemical homogeneity of both phases. Electron probe microanalysis (EPMA) was also performed to verify the chemical composition of the different phases of the composites. These measurements were performed using a CAMECA SX-100 instrument with an acceleration voltage of 20 kV and a probe current of 10 nA. Selected samples were used for X-Ray tomography using a Phoenix X-Ray Nanotom S system that enables obtaining a three-dimensional map of the distribution of the two phases within the volume of the sample. Data acquisition was realized at 90 kV acceleration voltage with a current of 90 μA for 153 min (6 x 750 ms acquisitions + 2 x

750 ms extinctions, for 1440 angular positions with steps of 0.25° and with an approximate resolution of 2 μm). The spatial reconstruction was performed with the open software ImageJ.

The three relevant transport properties were measured separately for each composition. Disk and bar-shaped samples were cut from the consolidated ingots with a diamond-wire saw. The thermal conductivity λ was obtained by measuring the thermal diffusivity a and the specific heat C_p of the composites. λ was then calculated following the formula $\lambda = a.C_p.\rho_v$ where ρ_v stands for the density, calculated from the weight and geometrical dimensions of the samples and considered temperature-independent. Thermal diffusivity was measured between 300 and 375 K on disk-shaped samples (10 mm in diameter and 1 mm in thickness) using the laser flash technique, with a LFA 427 system from Netzsch. C_p was measured under an Ar flow using a DSC 404 F3 Pegasus system from Netzsch according to the norm ASTM e967-11.

The electrical resistivity ρ and the Seebeck coefficient α were measured simultaneously from 300 up to 375 K with a ZEM-3 (ULVAC-RIKO) system on bar-shaped samples of typical dimensions of 1×1.5×8 mm^3.

III. Effective Medium Theory (EMT) and Generalized EMT for the thermoelectric properties

1). EMT and GEMT for the electrical and thermal conductivities

The effective medium theory (EMT) consists in a set of approximations that allow calculating the macroscopic properties of an inhomogeneous medium, based solely on the properties of the phases constituting the medium. For the interested reader, the

theoretical and historical bases of the EMT and the GEMT are described in the ESI (part B).

For the electrical conductivity σ and the thermal conductivity λ, the EMT theory leads to the following formula in the presence of two phases [12, 13]

$$\varphi_1 \frac{\sigma_1 - \sigma_e}{\sigma_1 + 2.\sigma_e} + \varphi_2 \frac{\sigma_2 - \sigma_e}{\sigma_2 + 2.\sigma_e} = 0 \quad (2)$$

$$\varphi_1 \frac{\lambda_1 - \lambda_e}{\lambda_1 + 2.\lambda_e} + \varphi_2 \frac{\lambda_2 - \lambda_e}{\lambda_2 + 2.\lambda_e} = 0 \quad (3)$$

where φ_1 and φ_2 are the volume fractions of the phases 1 and 2, respectively. The subscripts 1, 2 and e correspond to the phase 1, 2 and the effective medium, respectively.

The general effective medium theory formalism (based on a phenomenological model with the addition of elements of the percolation theory to the EMT [14, 15]) can be directly applied to the electrical and thermal conductivities, yielding the equations

$$\varphi_1 \frac{{\sigma_1}^{1/t} - {\sigma_e}^{1/t}}{{\sigma_1}^{1/t} + A.{\sigma_e}^{1/t}} + \varphi_2 \frac{{\sigma_2}^{1/t} - {\sigma_e}^{1/t}}{{\sigma_2}^{1/t} + A.{\sigma_e}^{1/t}} = 0 \quad (4)$$

$$\varphi_1 \frac{{\lambda_1}^{1/t} - {\lambda_e}^{1/t}}{{\lambda_1}^{1/t} + A.{\lambda_e}^{1/t}} + \varphi_2 \frac{{\lambda_2}^{1/t} - {\lambda_e}^{1/t}}{{\chi_2}^{1/t} + A.{\lambda_e}^{1/t}} = 0 \quad (5)$$

where all the constants are the same as described in Eqs. (2), and (3). In Eqs. (4) and (5), A is a constant that depends on the actual percolation threshold φ_c (of the phase 2 in the

phase 1) through the equation A = (1-φ_c)/φ_c, and t is a constant representing the asymmetry of the microstructure (in terms of connection between the grains).

2). EMT and GEMT for the thermopower

The thermopower appears as the last property to be described in multi-phased media to enable a direct estimation of the ZT values. In 2005 and 2006, Sonntag derived a formula valid for metals or degenerate semiconductors by applying the EMT formalism to the heat flux and chemical potential [16, 17]. Few years later, replacing the heat flux by the entropy flux, a more general equation was derived, thereby extending the previous model to non-degenerate semiconductors [18]. In this model, the quantity λ/α is used as χ and is introduced in Eq.(1) resulting in the following expression

$$\varphi_1 \frac{\frac{\lambda_1}{\alpha_1} - \frac{\lambda_e}{\alpha_e}}{\frac{\lambda_1}{\alpha_1} + 2.\frac{\lambda_e}{\alpha_e}} + \varphi_2 \frac{\frac{\lambda_2}{\alpha_2} - \frac{\lambda_e}{\alpha_e}}{\frac{\lambda_2}{\alpha_2} + 2.\frac{\lambda_e}{\alpha_e}} = 0 \qquad (6)$$

where α_1, α_2 and α_e are the thermopowers of the phases 1 and 2 and of the effective medium, respectively. This equation requires the knowledge of λ for a set of different volume fractions prior to calculating α. We then applied the GEMT formalism in the same fashion as for the two other properties by applying the equation

$$\varphi_1 \frac{\left(\frac{\lambda_1}{\alpha_1}\right)^{1/t} - \left(\frac{\lambda_e}{\alpha_e}\right)^{1/t}}{\left(\frac{\lambda_1}{\alpha_1}\right)^{1/t} + A.\left(\frac{\lambda_e}{\alpha_e}\right)^{1/t}} + \varphi_2 \frac{\left(\frac{\lambda_2}{\alpha_2}\right)^{1/t} - \left(\frac{\lambda_e}{\alpha_e}\right)^{1/t}}{\left(\frac{\lambda_2}{\alpha_2}\right)^{1/t} + A.\left(\frac{\lambda_e}{\alpha_e}\right)^{1/t}} = 0 \qquad (7)$$

where A and *t* are, respectively, the same percolation-depending and asymmetry constant as in Eq . (4).

3). Consequences on the figure of merit ZT

Using Eqs. (2) to (7), a theoretical estimation of ZT_e of a two-phased composite can be obtained, for a given volume fraction provided the transport properties of each phases are known. Based on this set of equations, several combinations of state-of-the-art thermoelectric materials can be tested to determine whether the ZT values can be further optimized within this approach. By dividing the equation for a general property χ (Eq.1) by either χ_1 or χ_2, the function χ_e/χ_2 (which is a function of the volume fraction of the second phase φ_2) only depends on the ratio χ_1/χ_2. In other words, the EMT equations can be reduced to the properties of one of the two phases

$$\varphi_1 \frac{\frac{\chi_1}{\chi_2} - \frac{\chi_e}{\chi_2}}{\frac{\chi_1}{\chi_2} + 2.\frac{\chi_e}{\chi_2}} + \varphi_2 \frac{1 - \frac{\chi_e}{\chi_2}}{1 + 2.\frac{\chi_e}{\chi_2}} = 0 \qquad (8)$$

This procedure can be extended to the three transport properties involved in the ZT calculation and to the GEMT equations. The shape of the ZT_e/ZT_2 curve then only depends on the three ratios σ_1/σ_2, λ_1/λ_2, and α_1/α_2 as well as on the two GEMT parameters *t* and φ_c. Using these reduced equations, we calculated the evolution of ZT as a function of each ratio to determine their influence.

Figure 2 displays the ZT evolution of a composite as a function of the volume fraction with different sets of transport properties ratios in the simpler EMT case (as shown and discussed in the ESI).. In the general case of the GEMT, the shape of the ZT curve is similar and only stretched in the vertical or horizontal direction. A first clear outcome is that the ratio of thermopowers seems to have the strongest influence on the maximum ZT while the ratio of thermal conductivities tends to shift the volume fraction at which this maximum occurs. However, what is more surprising is that the ratio of electrical resistivities does not seem to have any influence on the maximum ZT value within this model (see Figure C in Supporting information). This result is very counterintuitive, as one would expect a significant decrease in ZT when the lowest electrical resistivity increases. Whether or not a maximum in ZT exists is an essential issue that critically depends on the nature and thus, on the transport properties of the two phases. A systematic study with hundreds of different ratio combinations (always maintained within physical limits of the three properties) confirms those trends. Yet, it is worthwhile to note that in order to obtain an increase in ZT of only 50%, a thermopower ratio over 8 is needed. As a consequence, assuming that the phase 2 shows thermopower values around 100 μV/K, such ratio would then require a second phase exhibiting thermopower values of the order of 1000 μV/K, a value rarely achieved among known materials. Ratios lower than 2 have no effect on the maximum ZT. Furthermore, the higher the thermopower ratio is, the lower the required crystalline fraction is. This piece of information is particularly relevant regarding synthesis issues.

As for the thermal conductivity, no clear trend emerges from these calculations. This ratio affects mainly the position of the maximum, converging to 33% as the ratio decreases. Once more, in a very counterintuitive way, the presence of one phase with a very low thermal conductivity does not affect the final ZT but rather the volume fraction φ_2 at which the maximum occurs.

The fact that a maximum ZT higher than ZT_1 and ZT_2 is achieved may be rather surprising at first glance since this theory should normally yield results of effective properties that are bounded by the properties of the original phases. However, the difference in the evolution of ρ, λ and α as a function of the crystalline fraction gives rise to enhanced ZT values.

Taken as a whole, these results provide interesting insights into the transport properties the two phases should possess in order to possibly achieve higher ZT values. In the frame of this model, one phase should display large thermopower values together with low thermal conductivity while the second phase should show the opposite properties, that is, low thermopower and high thermal conductivity. In spite of the fact that the electrical resistivity of the first phase is expected to have virtually no influence, the electrical resistivity of the second phase should be low enough to reach high ZT_2 values. The former combination can be obtained by considering chalcogenide glasses, which exhibit extremely low thermal conductivity (< 0.3 W m^{-1} K^{-1}) due to the inherent structural disorder, and high thermopower values (>> 500 μV K^{-1}) [19].

IV. Experimental test of the models with glass-crystal composites

Because amorphous systems are usually thermally stable in a limited temperature range above room temperature, we prepared composite samples using a glassy Si-As-Te phase with crystalline Bi-Sb-Te compounds that show excellent thermoelectric properties near room temperature. This type of glassy system exhibits a very low vitreous transition temperature T_g. The chosen composition $Si_{10}As_{15}Te_{75}$ shows a T_g at 383 K (see ESI, Figure D).

A low-T_g glass exhibits the main advantage of facilitating the fabrication process. Above this characteristic temperature, the viscosity of the glass drastically decreases while maintaining its solid state. Hence, under pressure, it can then be severely strained. Mixing powders of the two phases, with heating and pressure, allows producing a composite of crystalline particles (phase 2) embedded in a glassy matrix (phase 1).

The composition of the crystalline phase was chosen in order to obtain a high contrast between both thermopower and thermal conductivity ratios. Moreover, the two phases are *p*-type, as this type is more easily obtained in chalcogenide glasses [20]. The properties of the two phases at 300 K as well as the corresponding ratios are summarized in Table 1.

Table 1: Properties of the two phases (crystalline $Bi_{0.4}Sb_{1.6}Te_3$ and glassy $Si_{10}As_{15}Te_{75}$) at room temperature, and ratio of the two properties as expressed in Section III. Properties of the $Bi_{0.4}Sb_{1.6}Te_3$ phase are described in both directions i.e. perpendicular (⊥) and parallel (//) to the pressing direction in SPS.

Phase type	$Bi_{0.4}Sb_{1.6}Te_3$ //	$Bi_{0.4}Sb_{1.6}Te_3$ ⊥	$Si_{10}As_{15}Te_{75}$	Ratio (vitreous/crystalline)
Electrical resistivity (μΩ.m)	10.1	7.3	$3.39\ 10^8$	$4.6\ 10^7$
Seebeck coefficient (μV/K)	+166	+ 164	+ 1400	8.5
Thermal conductivity (W/m.K)	1.1	1.4	0.17	0.12

Due to the well-known intrinsic anisotropy of Bi_2Te_3 compounds [21] clearly evidenced in $Bi_{0.4}Sb_{1.6}Te_3$ (Table 1), the composites may be expected to show some degree of anisotropy in their transport properties which might be a function of the crystalline fraction. For this reason, we carried out the calculations in both directions taking into account the ρ, α and λ values associated to each direction.

1). Characterization of the BiSbTe-SiAsTe composites

SEM analyses highlight a very poly-disperse and homogeneous distribution of the crystalline phase (light-grey phase) in all composites . Crystalline grains of few microns "connecting" larger grains could be observed. Although the crystalline powder was sieved at 25 μm, larger features are also present, emphasizing agglomeration of that

phase. An example of a set of SEM pictures for one of the composites (60-40%) is shown in the ESI (Figure F1). In addition, EPMA measurements (ESI, Figure F2) revealed a slight migration of Sb (around 1 at%) from the crystalline phase to the glassy phase.

In the classical EMT (ESI, part B), the percolation threshold is implicitly predicted to be around 33%. However, this is not to say that this value is indeed achieved in the present series of samples. To shed light on the possible actual percolation threshold, we performed X-ray tomography to determine the crystalline phase distribution in the sample's volume. Of note, it should be kept in mind that the spatial resolution of this technique is around 2 microns, while features at the micrometer and sub-micrometer scales are clearly observed (see Figure F1 in ESI). Hence, this method only allows setting an upper limit to the percolation threshold in the present case.

Figure 3 shows the reconstructed 3D maps of the crystalline phase in the composites with crystalline fractions of 10, 20 and 30%. The left-hand image (10%) clearly shows the absence of connection between the grains, while on the right-hand image (30%), clear connections between the grains are evidenced. In the last image (20%), the situation seems intermediate with connections between some grains and unconnected areas. Even though an exact determination of the percolation threshold is somewhat difficult, the actual percolation threshold in this series of composites is estimated to be below 20%. This estimation is consistent with the percolation theory which predicts a value between 15 and 17 % [22]. With such a constraint on φ_c, Eqs. (4),(5) and (7) of the GEMT can be used to fit the experimental data with t and φ_c as free parameters, at every measured temperature in the range 300 – 375K.

2). Comparison between the predictions of the GEMT model and the measured properties

Figure 4 displays the results of the fitting procedure for both the electrical resistivity and thermal conductivity at 300 and 375 K. The best fits to the data were obtained for t = 2 and φ_c = 16 % (a percolation threshold close to the 16.6 % predicted by the percolation theory) and are displayed in Figure 4A. From early fitting tests to the electrical resistivity, it was noticed that the experimental trend in ρ at the asymptotic limit (*i.e.* 100% crystalline fraction) was not in agreement with the value of 7 μΩ.m measured for $Bi_{0.4}Sb_{1.6}Te_3$. A possible origin of this discrepancy might be related to variations in the chemical composition of the crystalline phase. Chemical analyses indicated an enrichment of the glassy phase in Sb (normally not affecting its properties considering its very low concentration [19]), being indirectly a sign of Sb depletion in the original crystalline phase. As pointed out by Scherrer et al. [21], the evolution of the Bi/Sb ratio could be responsible for an increase in the electrical resistivity of that magnitude. A modified electrical resistivity for the crystalline phase (25 μΩ.m instead of 7 μΩ.m in the perpendicular direction, obtained from the asymptotic limit for a pure crystalline phase in the experimental data) was subsequently used in the calculations. As can be observed in Figure 4, the fitted curve matches very well the experimental data. For the thermal conductivity, the measured λ values of $Bi_{0.4}Sb_{1.6}Te_3$ were decreased accordingly using the Wiedemann-Franz law. However, the resulting fit still overestimates the measured data. As phonon diffusion at interfaces is not taken into account in EMT-type models and considering the microstructure of the composites, the reduction of the thermal conductivity by these mechanisms could result in such a decrease [23].

Regarding the prediction of the thermopower, the results obtained for the same set of t and φ_c parameters are shown in Figure 5. With these t and φ_c factors, the agreement between the measured and calculated data is far from being satisfactory. Even though the drop in α at low crystalline fractions is predicted, its magnitude is not well captured. Noteworthy, varying the fitting factors did not improve the quality of the fit.

3). Discussion on the prediction failure by EMT for the thermopower

Although the GEMT yielded some reliable results for both the electrical resistivity and thermal conductivity, this model clearly fails to predict the thermopower based on Sonntag's equation. One may argue that the formalism applied to ρ and λ in the GEMT may not be fully valid for λ/α. However, this discrepancy is likely more deeply rooted in the approximations of the model itself. Interfaces and/or microstructures might play an important role and are not taken into account in Sonntag's model. As for the derivation of the equations themselves, nothing can really be argued, not to mention their experimental validation on the conducting composite systems [17, 18]. However, having in mind the simple short circuit concept, it seems rather unphysical that electrical conductivity should not play any direct role in the equation of the thermopower for a composite system, especially with a combination of conducting and insulating components. Among all the thermopower models we subsequently compared to these results, the Webman Jortner and Cohen model [24] seemed the most adequate with a very different equation derivation (not based on Eq.1 contrarily to Sonntag's model), while remaining in the frame of the EMT.

4). Webman-Jortner-Cohen (WJC) model for the thermopower

Webman, Jortner and Cohen (WJC) derived a different equation for the thermopower by applying the EMT to Onsager equations. They assumed that corrections for both σ_e and λ_e are small due to thermoelectric effects [24, 25] and wrote α_e as follows:

$$\alpha_e = \frac{\langle \alpha\sigma/\Delta_0 \rangle}{\langle \sigma/\Delta_0 \rangle} \quad (9)$$

where $\Delta_0 = (2\sigma_e + \sigma)(2\kappa_e + \kappa)$. If the system is limited to two components, the development, in a similar way as the above-mentioned equations of the EMT, yields

$$\varphi_1 \frac{\sigma_1(\alpha_e - \alpha_1)}{(2\sigma_e + \sigma_1)(2\lambda_e + \lambda_1)} + \varphi_2 \frac{\sigma_2(\alpha_e - \alpha_2)}{(2\sigma_e + \sigma_2)(2\lambda_e + \lambda_2)} = 0 \quad (10)$$

where all the constants are as in part III. The limiting cases of this equation are well described by Snarskii et al. in Ref. [25]. In Figure 6, we present four cases for high and low electrical conductivity ratios, with thermopower and thermal conductivity ratios similar to those of our composites. These results are compared to those obtained with the model developed by Sonntag.

Considering the comparison presented in Figure 5, the WJC model seems more consistent with our experimental results than the Sonntag's model *i.e.* in the case of very high ρ_1/ρ_2 ratios. Both models agree only when this ratio is low. Compared to the experimental thermopower values obtained for our composites presented in Figure 5, the WJC model reproduces well the steep decrease followed by a plateau. However, the curve shape predicted by Eq.(10) suffers from the same drawbacks as the original EMT theory: the percolation threshold is irrevocably pinned at 33% while it can considerably

differ in real materials. Hence, we combined the WJC model within the framework of the GEMT by introducing the factors t and A in Eq.10, leading to the following equation:

$$\varphi_1 \frac{{\sigma_1}^{1/t}.({\alpha_e}^{1/t} - {\alpha_1}^{1/t})}{(A.{\sigma_e}^{1/t} + {\sigma_1}^{1/t})(A.{\lambda_e}^{1/t} + {\lambda_1}^{1/t})} + \varphi_2 \frac{{\sigma_2}^{1/t}.({\alpha_e}^{1/t} - {\alpha_2}^{1/t})}{(A.{\sigma_e}^{1/t} + {\sigma_2}^{1/t})(A.{\lambda_e}^{1/t} + {\lambda_2}^{1/t})} = 0 \quad (11)$$

Figure 7A presents the results obtained with Eq.11, using the t factor and percolation threshold φ_c previously obtained by fitting the electrical resistivity and thermal conductivity (*i.e.* t = 2 and φ_c = 16%). As can be seen, this modified equation accounts well for the variations in the thermopower and the ZT values as a function of the crystalline fraction (Figs. 7A and 7B).

The better match between experiment and theory obtained with the WJC model emphasizes that both electrical and thermal conductivity should be taken into account when modeling the Seebeck coefficient in composites. Yet, does this model leave room for enhanced ZT in composites? To answer this question, we tested numerically several combinations with transport properties and t and φ_c parameters spanning the range of physically meaningful values for thermoelectric composites (ρ_1/ρ_2 ranging from 0.1 to 10^4, α_1/α_2 from 0.1 to 20, λ_1/λ_2 from 0.01 to 10, t from 1 to 3 and φ_c from 10 to 50%). None of the combination tested led to an optimized ZT value. Thus, it can be safely concluded that within the frame of the GEMT equations, the association of two or more compounds with different thermoelectric properties cannot lead to enhanced ZT values. This is particularly clear when the electrical resistivity ratio is of several orders of

magnitude. This result follows the observations of Bergman [11], although this conclusion was reached in the present case using a very different theoretical framework. However, it should be underlined that these theoretical models uses some simplifications. More specifically, interface effects such as electron filtering (able to increase the thermopower in specific cases [21, 26, 27]), or the influence of thermoelectric effects on both the electrical resistivity and thermal conductivity (that may trigger peculiar phenomena close to the percolation threshold [25]) are not taken into account.

V. Conclusion

We reported on the modeling of the thermoelectric properties of two-phase composites using various models based on the effective medium theory. The predictions of these models were compared to experimental results obtained on crystalline phases of $Bi_{0.4}Sb_{1.6}Te_3$ embedded in a $Si_{10}As_{15}Te_{75}$ glassy matrix with various fractions. While the generalized version of the EMT predicts a maximum in ZT at a particular crystalline fraction, our results did not show such an increase. A modified version of the GEMT that includes the WJC equation was found to provide a better agreement between theory and experiment. This model enables predicting the transport properties of composite materials with two phases exhibiting high electrical and thermal conductivity contrasts. In addition, this model demonstrates that this approach yields no significant increase in ZT values, which agrees with the work of Bergman despite the different theoretical frameworks used. However, considering the huge interface effects on the thermal and electronic properties, and the behavior near percolation threshold, it cannot be ruled out that increased ZT values might be achieved in two- or more components

compounds. Crystalline-crystalline composite systems, for which Sonntag's equation still apply and for which electron filtering may occur, would be worth to be investigated to further test this model. Finally, the presented set of equations could be used to predict the limit at which secondary phases, frequently appearing in the synthesis process of thermoelectric materials, deteriorate significantly the transport properties.

Acknowledgements

The authors would like to thank financial support from the French National Agency (ANR) in the frame of its programme "PROGELEC" (Verre Thermo-Générateur "VTG"). We acknowledge C. Merlet and M. Boyer for their help in EPMA experiments, M. Bigot for help in glass synthesis and J. Couve for his help in the DSC measurements.

Figure captions

Figure 1. XRD patterns of glassy $Si_{10}As_{15}Te_{75}$ and crystalline $Bi_{0.4}Sb_{1.6}Te_3$ phases.

Figure 2. Evolution of ZT with the crystalline fraction of phase 2 embedded in a matrix (phase 1), with different ratios of the Seebeck coefficient and the thermal conductivity (see the ESI concerning the ratios of the electrical resistivity).

Figure 3. X-ray tomography reconstruction of a sample volume (typically 4x0.5x0.5 mm^3) for three different composites.

Figure 4. Electrical resistivity (A) and thermal conductivity (B) of the BiSbTe-SiAsTe composites at 300 and 375K. The measured data are represented by the dots while the solid curves represent the calculated data with φ_c = 16 % and t =2.

Figure 5. Thermopower of the BiSbTe-SiAsTe composites measured at 300 and 375 K. The measured data are represented by the dots while the solid curves represent the calculated data with φ_c = 16% and t =2.

Figure 6. Predicted evolution of the thermopower with the crystalline fraction for α_1/α_2 = 5 and λ_1/λ_2=0.2 inferred from the Sonntag equation (in red) and the WJC equation (in blue) for various resistivity ratios. Agreement between the two models is only reached for low ρ_1/ρ_2 ratios. The WJC model better reproduces the shape of the experimental curve shown in Fig. 5.

Figure 7. (A) Comparison between the results of the WJC model for the thermopower (green solid line) and the same model coupled with the GEMT principles (red dashed line), for the SiAsTe-BiSbTe composites (experimental results are shown by red dots). (B) Results obtained for the ZT, using Eqs. 4, 5 and 11 for the electrical conductivity, thermal conductivity and thermopower, respectively. The solid and dashed blue lines correspond to the simulation made with the properties measured perpendicular and parallel to the pressing directions, respectively, of the crystalline $Bi_{0.4}Sb_{1.6}Te_3$ phase. Red squares stand for the experimental values. The slight under-estimation of ZT observed for φ_1>35% stems from the over-estimation of λ owing to interface effects.

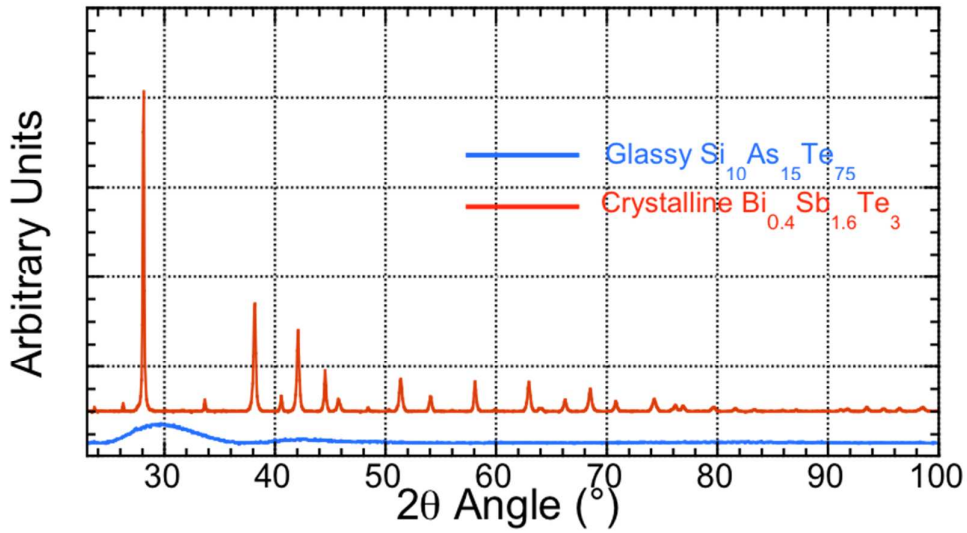

Figure 1

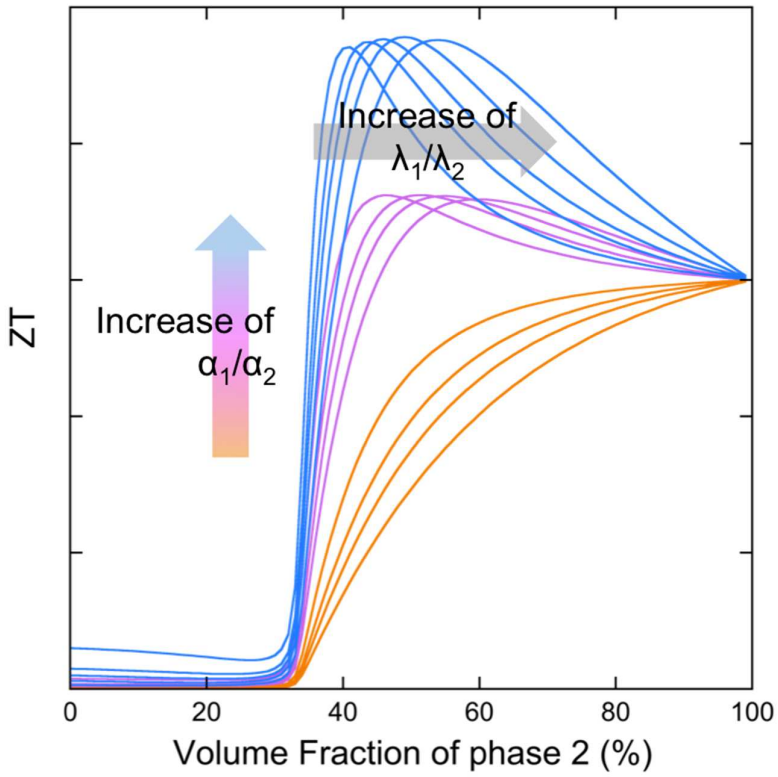

Figure 2

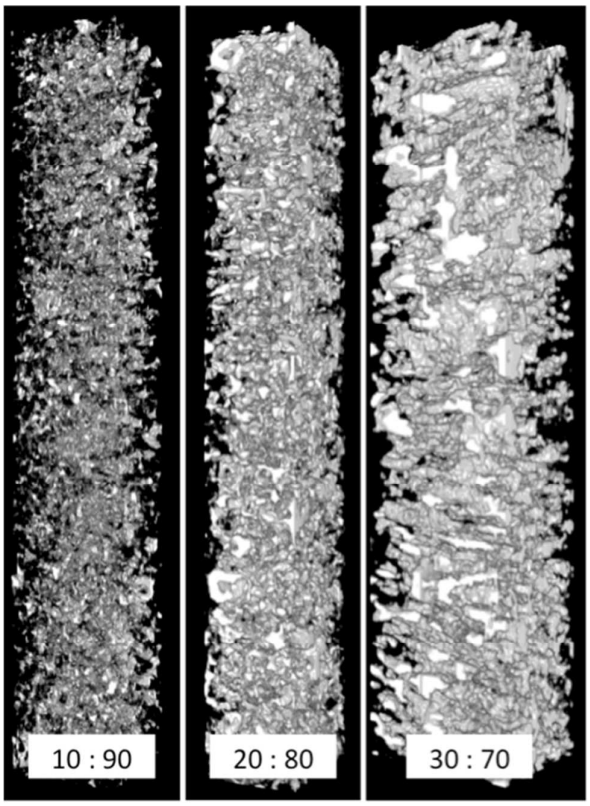

Figure 3

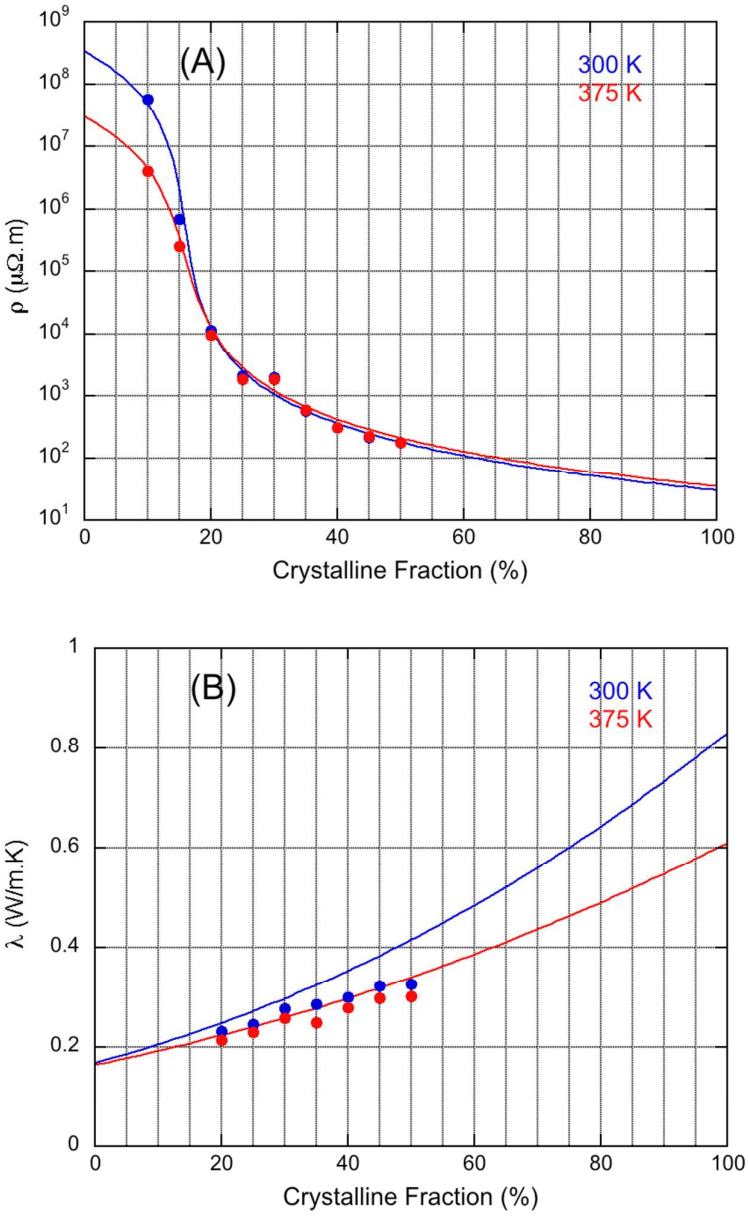

Figure 4

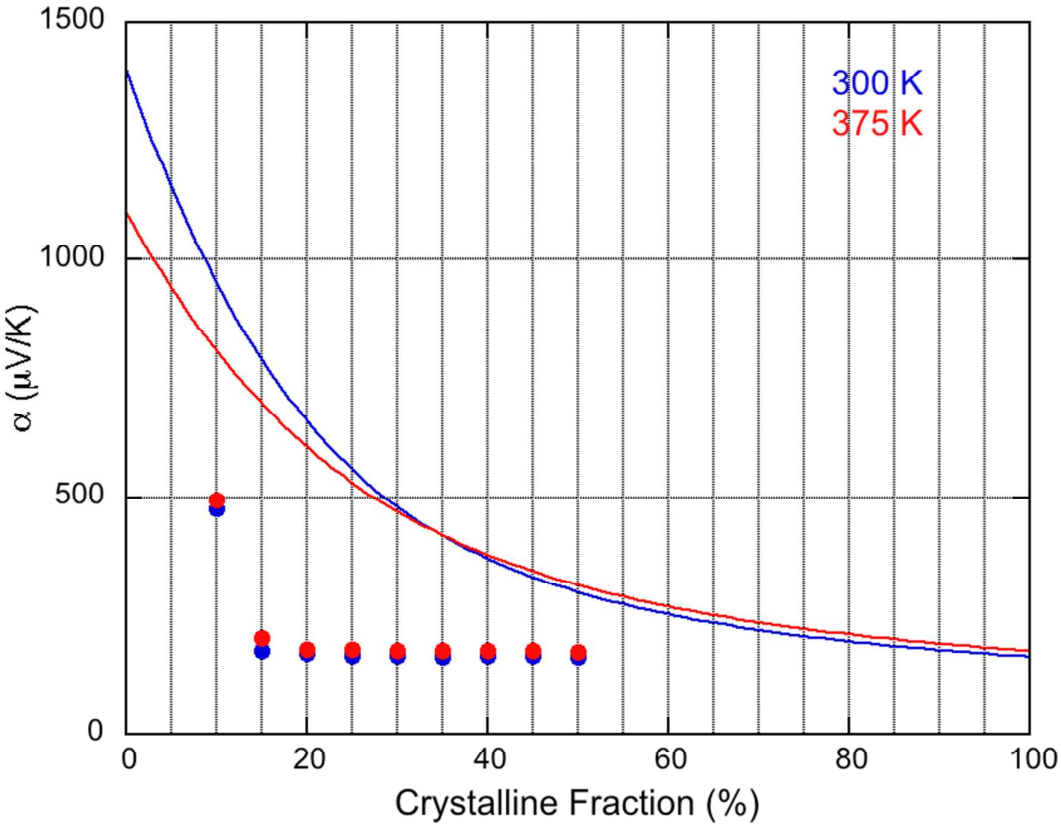

Figure 5

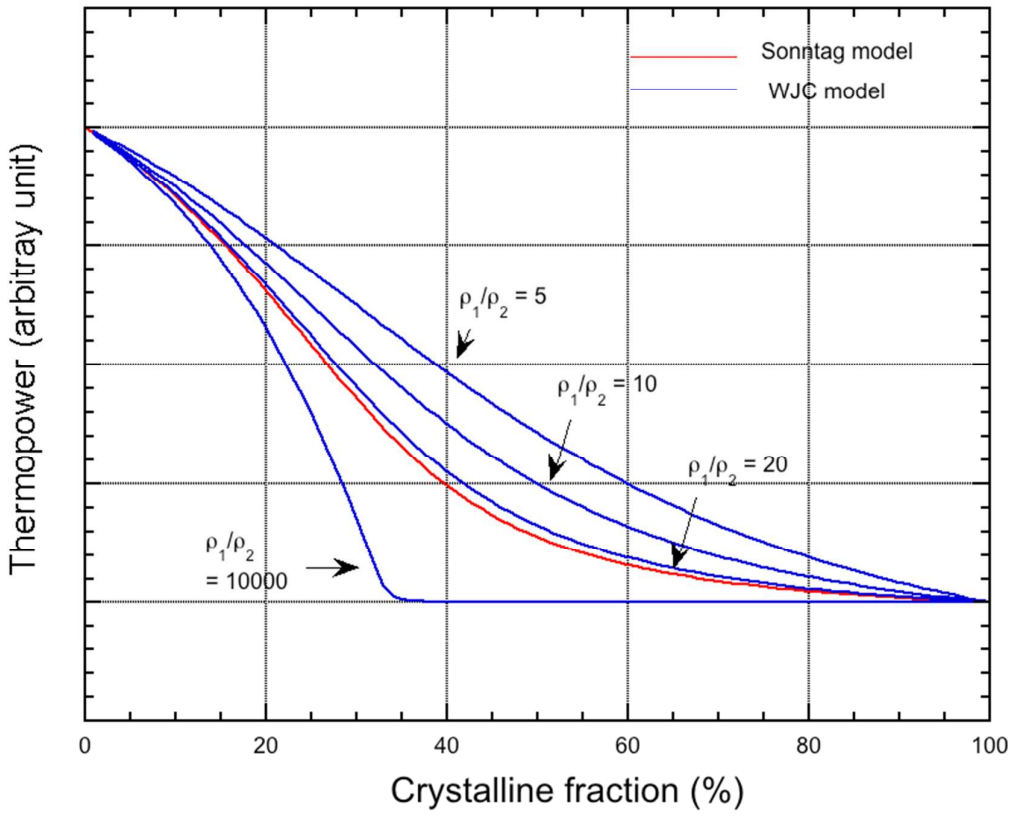

Figure 6

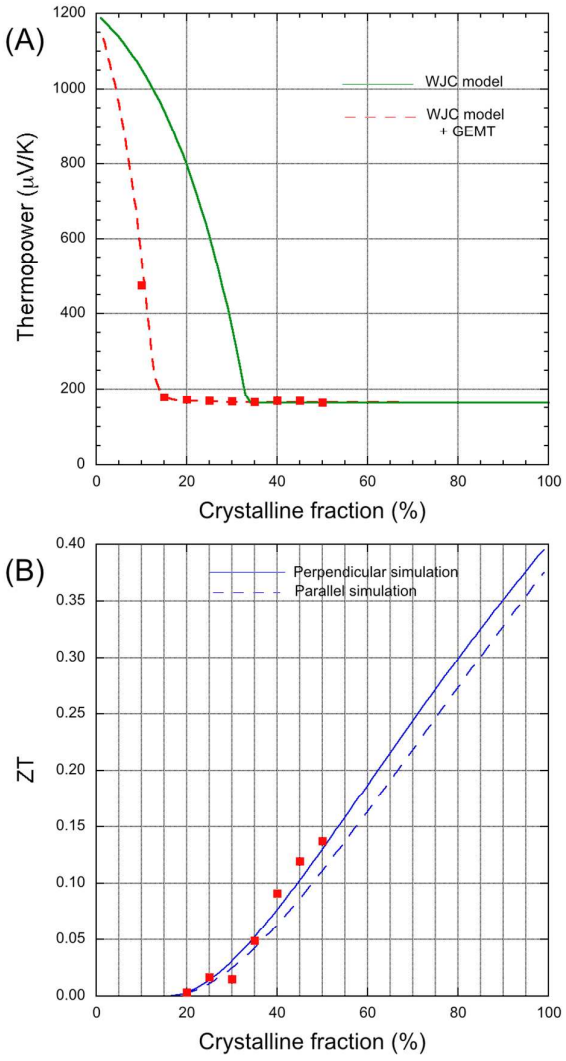

Figure 7

References

1. L. D. Hicks and M. S. Dresselhaus, *Phys. Rev. B*, 1993, **47**, 12727-12731.
2. G. Nolas, G. Slack, D. Morelli, T. Tritt and A. Ehrlich, *J. Appl. Phys.*, 1996, **79**, 4002-4008.
3. K. Biswas, J. He, I. D. Blum, C.-I. Wu, T. P. Hogan, D. N. Seidman, V. P. Dravid and M. G. Kanatzidis, *Nature*, 2012, **489**, 414-418.
4. Y. Lee, S.-H. Lo, J. Androulakis, C.-I. Wu, L.-D. Zhao, D.-Y. Chung, T. P. Hogan, V. P. Dravid and M. G. Kanatzidis, *J. Am. Chem. Soc.*, 2013, **135**, 5152-5160.
5. D. G. Zhao, M. Zuo, Z. Q. Wang, X. Y. Teng and H. R. Geng, *J. Nanosci. Nanotechnol.*, 2015, **15**, 3076-3080.
6. J. Wang, X. X. Ye, X. B. Yaer, B. Y. Zhang, W. Ma and L. Miao, *Scripta Mater.*, 2015, **99**, 25-28.
7. J. Li, Q. Tan, J.-F. Li, D.-W. Liu, F. Li, Z.-Y. Li, M. Zou and K. Wang, *Adv. Funct. Mater.*, 2013, **23**, 4317-4323.
8. J. Lingner, M. Letz and G. Jakob, *J. Mater. Sci.*, 2012, **48**, 2812-2816.
9. J.-B. Vaney, G. Delaizir, E. Alleno, O. Rouleau, A. Piarristeguy, J. Monnier, C. Godart, M. Ribes, R. Escalier, a. pradel, A. Goncalves, E. Lopes, G. J. Cuello, P. Ziolkowski, E. Mueller, C. Candolfi, A. Dauscher and B. Lenoir, *J. Mater. Chem. A*, 2013, **1**, 8190-8200.
10. J. B. Vaney, G. Delaizir, E. Alleno, O. Rouleau, A. Piarristeguy, J. Monnier, C. Godart, M. Ribes, R. Escalier, A. Pradel, A. P. Goncalves, E. B. Lopes, G. J. Cuello, P. Ziolkowski, E. Muller, C. Candolfi, A. Dauscher and B. Lenoir, *J. Mater. Chem. A*, 2013, **1**, 8190-8200.
11. D. J. Bergman and L. G. Fel, *J. Appl. Phys.*, 1999, **85**, 8205-8216.
12. R. Landauer, *J. Appl. Phys.*, 1952, **23**, 779-784.
13. V. Odelevskii, *Zh. Tekh. Fiz*, 1951, **21**, 678-685.
14. D. S. McLachlan, *J. Phys. C Solid State*, 1987, **20**, 865.
15. D. S. McLachlan, M. Blaszkiewicz and R. E. Newnham, *J. Am. Ceram. Soc.*, 1990, **73**, 2187-2203.
16. J. Sonntag, *Phys. Rev. B*, 2005, **71**.
17. J. Sonntag, *Phys. Rev. B*, 2006, **73**.
18. J. Sonntag, *J Phys Condens Matter*, 2009, **21**, 175703.
19. N. F. Mott and E. A. Davis, *Electronic processes in non-crystalline materials*, Oxford University Press, 1982.
20. A. Kolobov, *J. Non-Cryst. Solids*, 1996, **198**, 728-731.
21. D. M. Rowe, *Thermoelectrics handbook: macro to nano*, CRC press, 2006.
22. A. Aharony and D. Stauffer, *Introduction To Percolation Theory*, Taylor & Francis, 2003.
23. C. M. Bhandari and D. M. Rowe, *J. Phys. C Solid State*, 1978, **11**, 1787.
24. I. Webman, J. Jortner and M. H. Cohen, *Phys. Rev. B*, 1977, **16**, 2959-2964.
25. A. Snarskii and I. Bezsudnov, *J. Thermoelec.*, 2005, **3**, 7.
26. J.-H. Bahk, Z. Bian and A. Shakouri, *Phys. Rev. B*, 2013, **87**, 075204.
27. Y. Zhang, J.-H. Bahk, J. Lee, C. S. Birkel, M. L. Snedaker, D. Liu, H. Zeng, M. Moskovits, A. Shakouri and G. D. Stucky, *Adv. Mater.*, 2014, **26**, 2755-2761.

An experimental and modeling study of glass-crystal $Si_{10}As_{15}Te_{75}$-$Bi_{0.4}Sb_{1.6}Te_3$ composites using various improved equations of the effective medium theory.

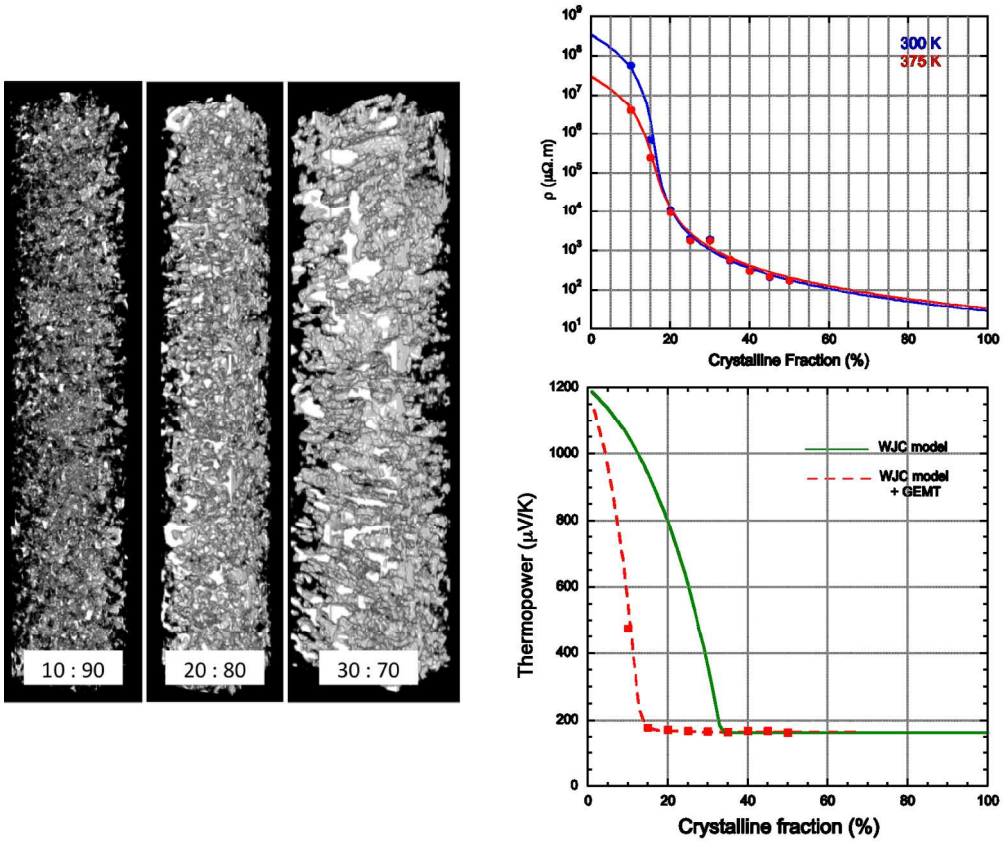

302x256mm (150 x 150 DPI)